We sincerely thank you for your valuable comments and constructive suggestions. We have substantially revised the manuscript to address all the concerns raised in the review. First, we strengthened the evaluation and mechanistic analysis of the simulated cloud and precipitation responses. Second, we clarified the treatment of the annual PV datasets and the paired experimental design, and further evaluated the radiative parameterization and surface energy balance closure. Third, we clarified the distinction between WRF-PV and previous modeling approaches by conducting an additional effective albedo experiment and directly comparing the different implementations. Fourth, we expanded the discussion of ecosystem processes and their implications for future model development. In addition, in response to another reviewer's comments, we updated the WRF physical configuration and adopted the higher-resolution CLDAS dataset. We then repeated the simulations and diagnostic analyses and redrew the figures. Detailed responses to each of these concerns are provided below.

Comment 1: *Line 155: A major concern is the consistency and potential bias introduced by merging multiple PV datasets with different temporal coverages (2013–2023 vs. 2019–2022 vs. 2024) and classification methodologies. The manuscript does not clearly explain how discrepancies among these sources (e.g., spatial overlap, differing detection accuracies, or temporal mismatches) were reconciled into a unified PV distribution. In addition, filtering out installations smaller than 1 km² to match MODIS resolution may systematically exclude a large fraction of PV capacity, potentially biasing the spatial representation and subsequent analysis. The authors may clarify the data harmonization process and assess how these choices affect the robustness of their results.*

Response: Thank you for this comment. We have revised Section 3.2 to clarify the temporal coverage and spatial formats of the three PV datasets, the selection of the annual PV maps, and the spatial consistency across dataset transitions. The Photovoltaic Dataset of China covers 2013–2023 with a five-year temporal frequency and is provided as PV polygon vector data. We used its 2018 and 2023 layers. The Global Photovoltaic Solar Panel Dataset provides annual 20 m raster PV maps for 2019–2022. The China Photovoltaic Power Plant Vector Dataset provides the 2024 PV map as PV polygon vector data. Therefore, for the 2018–2024 simulations, only one annual PV map was available for each simulation year, and no same-year fusion or treatment of cross-dataset spatial overlap was required. All three datasets were derived from high-resolution satellite imagery using machine-learning-based methods and validated against manually interpreted reference samples, providing a common basis for quality assurance.

We also assessed the spatial consistency across dataset transitions. After applying a 100 m spatial tolerance, the lost area accounted for only 0–2.56 % of the total PV area in each year. This small proportion indicates that the prescribed PV maps maintained strong spatial continuity across adjacent years and showed few artificial discontinuities.

Across the 2018–2024 PV maps, PV installations smaller than 1 km² accounted for no more than 7.5 % of the total PV area in any year, indicating that the filtering retained the dominant share of PV-covered area throughout the study period. To further address the exclusion of smaller PV installations, future simulations can be conducted at higher spatial resolutions with increased computational resources and higher-resolution PV datasets. In parallel, we are currently conducting deep-learning-based research to investigate PV effects under finer and more realistic spatial scenarios.

The revised text reads:

> "Three datasets were used to characterize the spatial distribution of PV installations. The first was the Photovoltaic Dataset of China, which covers 2013–2023 at five-year intervals and is provided as PV polygon vector data (Lin, 2024). We used its 2018 and 2023 layers. The second was the Global Photovoltaic Solar Panel Dataset, which provides annual 20 m raster PV maps for 2019–2022 (Li et al., 2025a). The third was the China Photovoltaic Power Plant Vector Dataset, which provides the 2024 PV map as PV polygon vector data (Yang et al., 2025). All three datasets were based on high-resolution satellite imagery, generated using machine learning classification approaches, and validated against manually interpreted samples. For each simulation year, only one PV dataset was used to prescribe the PV distribution. To assess the spatial consistency across dataset transitions, the PV distributions in adjacent years were compared using a 100 m spatial tolerance. The lost area accounted for only 0–2.56 % of the total mapped PV area, indicating generally good spatial continuity across adjacent years. To align with the spatial resolution of the MODIS land surface temperature dataset, only PV facilities with areas greater than 1 km^2 were retained. Across the 2018–2024 PV maps, PV installations smaller than 1 km^2 accounted for no more than 7.5 % of the total PV area in any year, indicating that the filtering retained the dominant share of PV-covered area throughout the study period. The total mapped PV installation area increased from 205.68 km^2 in 2018 to 720.19 km^2 in 2024."

Location: Section 3.2, lines 190–203.

***Comment 2:** Line 180: While WRF_PV includes the "annual evolution" of PV distribution, it is still unclear whether WRF_CTL uses time-invariant land-use and how interannual variability is separated from PV-induced signals. Without a clear description of how PV changes are synchronized with the meteorological forcing and how differences are aggregated across years, the attribution of climate responses specifically to PV installations may be confounded. I suggest clarifying whether both experiments use identical atmospheric boundary conditions for each year, how PV expansion is implemented year by year, and whether sensitivity tests were performed to isolate PV effects from natural variability.*

Response: Thank you for this helpful comment. We have clarified the experimental design and aggregation procedure. WRF_PV and WRF_CTL were conducted as paired single-member sensitivity simulations for each summer from 2018 to 2024. The two experiments used identical meteorological initial and boundary conditions, physical parameterization schemes, and non-PV land-surface conditions. Thus, the two simulations differed only in the treatment of PV installations. In WRF_PV, PV expansion was represented through year-specific PV maps. For each year, the corresponding PV map was kept fixed throughout the summer simulation, consistent with the temporal resolution of the available datasets. In WRF_CTL, the original land-use field was held constant throughout 2018–2024, with no PV installations prescribed.

To isolate the PV-induced effects from natural variability, the analysis was based on the paired differences between WRF_PV and WRF_CTL. At each hour of the diurnal cycle, the difference from each day was treated as one sample, and a t-test was used to assess whether the mean difference was statistically significant.

The revised text reads:

"Two sets of WRF simulations were conducted to assess the climatic response to utility-scale PV installations during summer, when solar radiation is strong and land–atmosphere coupling has been shown to play an important role in East Asian climate (Zhang et al., 2011). The first experiment (WRF_PV) incorporated a year-specific PV distribution, while the second experiment (WRF_CTL) used the original land-use data without PV installations. WRF_PV and WRF_CTL used identical initial and lateral boundary conditions and the same physical parameterization configuration described in Section 3.3. For each simulation year, the corresponding annual PV map was kept fixed throughout the simulation period in WRF_PV, consistent with the annual temporal resolution of the available PV datasets. The utility-scale PV areas were converted into a binary PV grid mask on the WRF D03 grid. A WRF grid cell was identified as a PV grid cell if it intersected with the PV area. In WRF_PV, the PV-ground coupling scheme updated surface temperature and energy fluxes at PV grid cells and enabled an explicit representation of PV-atmosphere feedback. Each simulation ran separately for the period of 2018–2024, with simulations initialized on 1 May and terminated on 31 August. The first month (May) was discarded as the model spin-up period, while the remaining three months (June–August) were used for analysis."

Location: Sections 3.4 and 4.2, lines 226–237, 323 – 325.

Comment 3: *Line 265: The authors attribute the large increase in net radiation primarily to reduced SWup and LWup, yet it is unclear whether these magnitudes are consistent with realistic PV albedo, emissivity, and panel orientation assumptions. In particular, the role of specular reflection and its parameterization in the model is not sufficiently described, raising questions about whether the shortwave radiative behavior of PV panels is accurately represented. It would be helpful if the authors provided a clearer description and validation of the radiative parameterization (including albedo, emissivity, and angular dependence) and demonstrated that surface energy balance closure is maintained under these large flux changes.*

Response: Thank you for this important comment. In WRF-PV, the front-surface reflectance is calculated from the Fresnel law as a function of the solar incidence angle, following Duffie and Beckman (2013). The incidence angle accounts for the solar zenith angle, solar azimuth angle, panel tilt, and panel azimuth. In the present simulations, the panels were represented as fixed-tilt arrays with a tilt angle of 37° and a south-facing azimuth of 0° based on an in situ observation (Jiang et al., 2021).

As an observational consistency check, we compared the simulated daytime albedo over the PV grid cells with available field observations. The daytime value decreased from approximately 0.224 in WRF_CTL to approximately 0.140 in WRF_PV. This is consistent with Ying et al. (2023), who reported mean broadband shortwave albedo values of 0.22 at a nearby Gobi Desert site and 0.14 at a PV site. The observed PV-site albedo was also higher in the early morning and late afternoon, consistent with the angle-dependent Fresnel formulation. For emissivity, the prescribed front- and rear-surface emissivities are 0.82 and 0.97, respectively, following the measurements of Heusinger et al. (2020). Sun et al. (2017) similarly reported an emissivity of approximately 0.82 for commercial solar glass.

In the revised manuscript, we added a closed energy-budget table in Section 4.3 for WRF_CTL and WRF_PV. The energy-balance residual was calculated as:

$$\text{Residual} = \text{NetRad} - (\text{SH} + \text{LH} + \text{GRDFLX} + \text{Pout}).$$

Table R1 shows that the residual remained small compared with the major energy fluxes. In WRF_CTL, the residuals were −5.35, 0.06, and −2.64 W m^{-2} during daytime, nighttime, and over the full diurnal cycle, respectively. The corresponding residuals in WRF_PV were 2.92, 4.73, and 3.83 W m^{-2}. This result indicates that the implemented PV–ground energy-balance scheme maintained approximate numerical energy closure.

Table R1: Daytime, nighttime, and 24 h mean surface energy budget components over the WRF PV grid cells. All values are in W m^{-2}. (Table 2 in the revised manuscript)

Period	Experiment	NetRad	SH	LH	GRDFLX	Pout	Sum of terms	Residual
Daytime	WRF-CTL	282.70	164.58	43.01	80.46	0.00	288.05	−5.35
Daytime	WRF-PV	341.05	214.55	36.86	64.05	22.67	338.13	2.92
Nighttime	WRF-CTL	−66.58	−3.88	5.85	−68.60	0.00	−66.63	0.06
Nighttime	WRF-PV	−63.18	−20.30	5.63	−53.41	0.16	−67.91	4.73
24 h mean	WRF-CTL	108.06	80.35	24.43	5.93	0.00	110.71	−2.64
24 h mean	WRF-PV	138.93	97.13	21.24	5.32	11.41	135.11	3.83

The revised text reads:

" $\alpha_{PV,top}$ denotes the albedo of the front PV surface, calculated from the Fresnel law as an angle-dependent reflectance. "

"Table 2 summarizes the daytime, nighttime, and 24 h mean surface energy budgets over the WRF PV grid cells. The energy balance residual was calculated as the difference between net radiation and the sum of sensible heat flux, latent heat flux, ground heat flux, and electrical power output. In WRF_CTL, the residuals were −5.35, 0.06, and −2.64 W m^{-2} during daytime, nighttime, and over the full diurnal cycle, respectively. The corresponding residuals in WRF_PV were 2.92, 4.73, and 3.83 W m^{-2}. This result indicates that the implemented PV–ground energy-balance scheme maintained approximate numerical energy closure."

Location: Sections 2.1 and 4.3, lines 112–113, 372–377; Tables 1 and 2.

Comment 4: *Line 355: The discussion is not rigorously demonstrated. Other factors, such as differences in model configuration, domain size, resolution, boundary conditions, or background climate regimes, can also contribute to the discrepancy with previous studies. Without controlled sensitivity experiments (e.g., toggling only albedo treatment while keeping other processes identical), it is difficult to isolate which mechanisms drive the reduced magnitude of impacts, right? Some sensitivity tests should be considered. While the WRF-PV model is described as more physically realistic, the claim that it produces results "closer to observations" is not sufficiently justified, particularly for land-atmosphere interactions.*

Response: Thank you for this constructive suggestion. We agree that differences among previous studies may reflect multiple factors in addition to the PV representation. We therefore conducted a WRF_EA experiment replacing the physically based WRF-PV scheme with the effective albedo formulation of Li et al. (2018). All other model settings, simulation periods, meteorological forcing, and annual PV distributions were unchanged. The only difference was the representation of PV installations, with a constant effective albedo of 0.15 prescribed over the PV grid cells. WRF_EA produced a TSK bias of +2.62 °C and an RMSE of 4.02 °C relative to MODIS, both larger than those of WRF_PV and WRF_CTL, and it increased TSK relative to WRF_CTL, whereas WRF_PV produced daytime surface cooling. WRF_EA also yielded larger T2 and precipitation RMSEs. Further details are provided in Supplementary Text S2 and Table S1.

The revised text reads:

> "To compare WRF-PV with the effective albedo (EA) method of Li et al. (2018), we conducted an additional experiment (WRF_EA) in which the WRF-PV scheme was replaced by the EA method. The model domain, simulation period, and physical configuration remained unchanged. Details of the experimental design and the complete evaluation results are provided in Supplementary Text S2. WRF_EA produced a mean TSK bias of +2.62 °C and an RMSE of 4.02 °C, both larger than those of WRF_PV (−0.34 and 2.56 °C) and WRF_CTL (+0.70 and 3.07 °C). Relative to WRF_CTL, WRF_EA increased TSK, whereas WRF_PV produced daytime surface cooling. The warming simulated by WRF_EA contrasts with the daytime cooling reported by previous satellite-based studies of utility-scale PV farms (Zhang and Xu, 2020; Fan and Huang, 2021; Li et al., 2021; Wang et al., 2024; Xu et al., 2024). These contrasting responses highlight the limitations of representing PV installations solely through the bulk albedo of the entire grid cell. The EA method does not account for shading and the associated changes in ground heat storage. By contrast, WRF-PV explicitly represented panel coverage, panel thermal properties, and shading effects, and showed closer agreement with MODIS."

Location: Section 5, lines 470–480; Supplementary Text S2 and Table S1.

Comment 5: *Line 355: Given that the study highlights differences in cloud fraction and precipitation characteristics (including extremes), more rigorous validation against observational or reanalysis datasets is needed. This is especially important because precipitation redistribution (rather than total change) is a central conclusion.*

Response: Thank you for this helpful comment. We replaced the original precipitation box plot with spatial analyses of summer mean precipitation and accumulated extreme precipitation, together with the daily precipitation distributions (Fig. R1). The revised results show little change in domain-mean precipitation but clear spatial heterogeneity, including localized changes in extreme precipitation. Both the spatial precipitation response and the shift in the daily precipitation distribution showed broad similarity to the corresponding interperiod changes in the reanalysis dataset (Figs. R2–R3). Although these changes also contain signals of long-term climate change, the observed similarities partly support the simulated PV-related precipitation redistribution. To investigate the mechanism underlying this redistribution, Fig. R4 examines the PV-induced changes in sensible heat flux, low-level convergence, moisture convergence, and vertical motion. These changes were spatially coherent with the precipitation response, suggesting that PV-induced sensible heating, together with terrain-related ascent, contributed to the localized precipitation enhancement. As the conclusion focuses on the reduction in downward shortwave radiation, we added a corresponding interperiod analysis using the reanalysis dataset. The later period also showed reduced downward shortwave radiation, consistent with the direction of the simulated radiative response. The low-cloud increase is therefore discussed as a model-diagnosed mechanism contributing to this radiative response (Table R2).

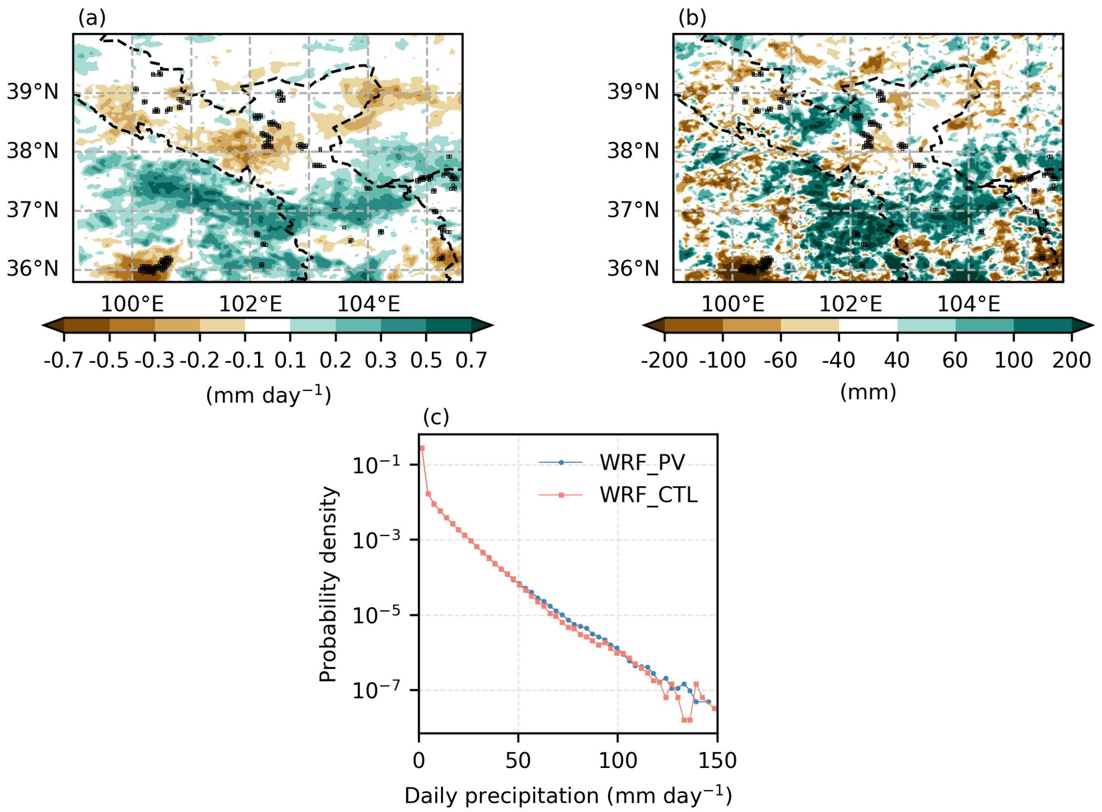

Figure R1: Spatial changes and probability density distributions of summer precipitation during 2018–2024. (a) Difference in mean daily precipitation between WRF_PV and WRF_CTL. (b) Difference in cumulative extreme precipitation (>30 mm day^{-1}) amount between WRF_PV and WRF_CTL. (c) Probability density distributions of daily precipitation intensity in WRF_PV and WRF_CTL over D03. In (a) and (b), grey grid symbols denote PV grid cells. (Figure 9 in the revised manuscript)

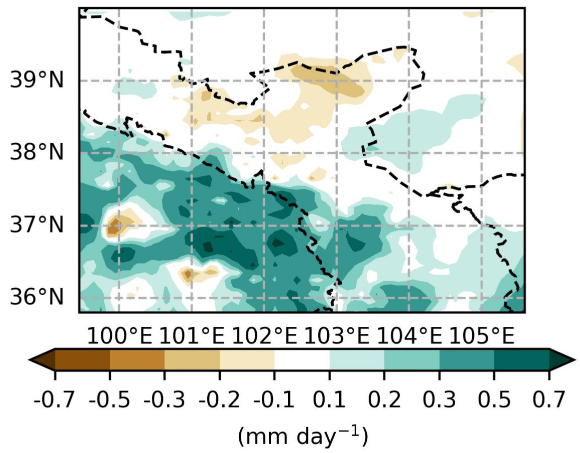

Figure R2: Difference in CMFD summer mean daily precipitation between 2018–2024 and 2000–2012. (Figure S1 in the supplement)

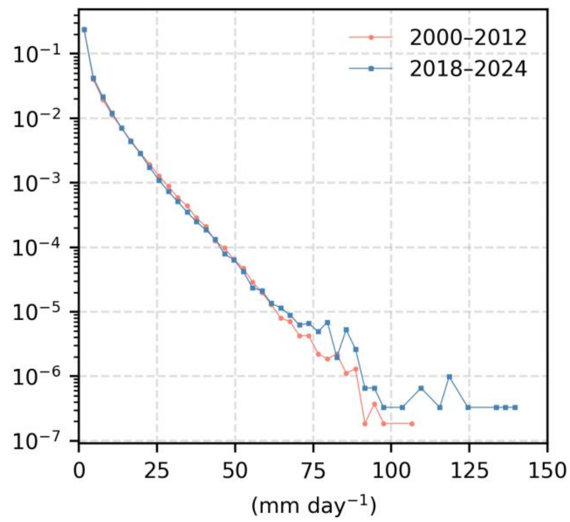

Figure R3: Probability density distributions of CMFD daily summer precipitation during 2000–2012 and 2018–2024. (Figure S2 in the supplement)

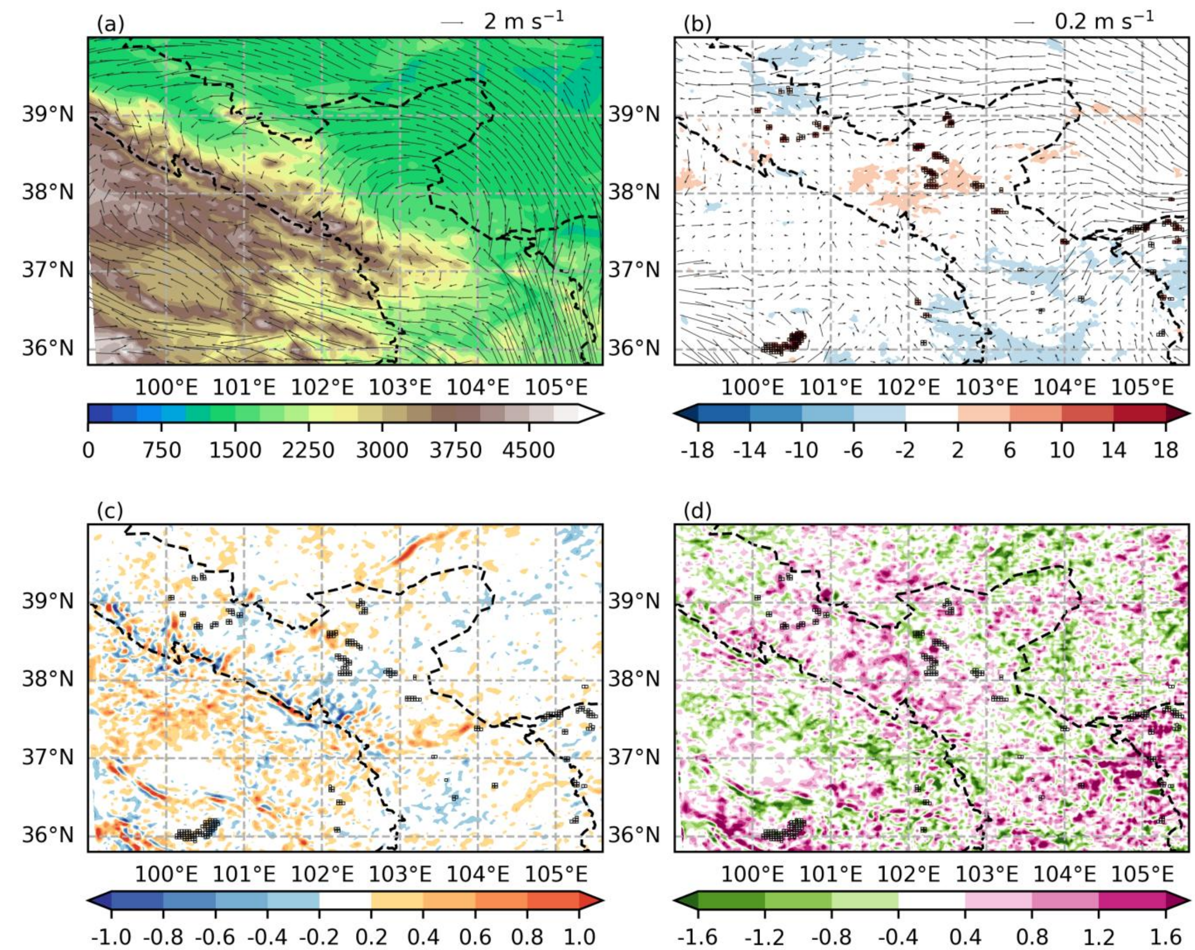

Figure R4: Terrain and atmospheric processes during the summers of 2018–2024. (a) Terrain height (m, shading) and near-surface wind field in WRF_CTL (vectors). (b) Differences in sensible heat flux (W m^{-2}, shading) and near-surface wind field (vectors). (c) Difference in vertical velocity (cm s^{-1}), with positive values indicating enhanced upward motion. (d) Difference in vertically integrated water vapor flux divergence (10^{-5} kg m^{-2} s^{-1}), with negative values indicating enhanced moisture convergence. All differences are calculated as WRF_PV minus WRF_CTL. In (b–d), grey grid symbols denote PV grid cells.

(Figure 10 in the revised manuscript)

Table R2: Comparison of summer mean downward shortwave radiation between 2000–2012 and 2018–2024 based on CMFD. (Table S2 in the supplement)

Variable	2000–2012	2018–2024	Difference (later − earlier)	p value
Summer mean downward shortwave radiation (W m^{-2})	257.06	249.77	−7.29	0.047

The revised text reads:

"Figure 9 shows the spatial distributions of the changes in daily mean and cumulative extreme precipitation between WRF_PV and WRF_CTL together with the probability density distributions of daily precipitation. The domain-mean precipitation difference between WRF_PV and WRF_CTL was small, indicating little change in the overall summer precipitation amount (Fig. 9a). However, the spatial response was pronounced, with precipitation increasing mainly over the central and southern parts of the domain and decreasing over several northern and western areas. Despite only small changes in mean precipitation (Fig. 9a), the related changes in water vapor convergence, vertical motion, and precipitation were dynamically coherent (Fig. 10c and 10d). This precipitation response pattern was broadly consistent with the period difference in the reanalysis data (Fig. S1). Accumulated extreme precipitation showed a more distinct and localized spatial response than mean precipitation (Fig. 9b). The probability distributions of WRF_PV and WRF_CTL were generally similar for light and moderate rainfall. However, WRF_PV showed a slightly higher probability density for heavy rainfall of 60–100 mm day^{-1}, suggesting a modest shift toward more intense rainfall events (Fig. 9c). A broadly similar shift in the daily precipitation distribution was also evident between the two periods in the reference dataset (Fig. S2)."

"In order to understand the association of the changes in circulation and precipitation with the PV distribution, Figures 10a and 10b show the summer-mean low-level circulation and the change in sensible heat caused by PV deployment. The climatological low-level flow was predominantly southeasterly and closely influenced by the regional topography (Fig. 10a). The climatological precipitation field exhibited pronounced spatial heterogeneity, with higher precipitation over the plateau, where the low-level flow encountered rising terrain (Fig. 3a and 10a). Between 36° and 37° N, PV-induced sensible heating strengthened low-level convergence, accompanied by an enhanced easterly flow and water vapor transport toward the plateau (Fig. 10b). This circulation anomaly reinforced the existing terrain-related convergence and ascent (Fig. 10c and 10d), contributing to increased precipitation over northern Qinghai. Moreover, we take the area of extreme precipitation near 38.6° N, which is located well within the model domain and is largely free from lateral boundary effects, as an example (Fig. 9b). Increases in sensible heat flux were concentrated over the PV clusters and were accompanied by convergence in the low-level wind field (Fig. 10b). The easterly, southeasterly, and northeasterly wind anomalies flowed toward the PV clusters and ascended along the mountain range that marks the northern boundary of Gansu Province (Fig. 10a), inducing weak upward motion (Fig. 10c). Although this weak anomalous ascent led to only a slight modification of mean precipitation (Fig. 9a), it could produce enhanced extreme precipitation under appropriate conditions (Fig. 9b). These spatial correspondences suggested that PV-induced increases in sensible heat flux perturbed the local circulation, while the background flow and complex terrain modulated the locations of the resulting ascent, moisture convergence, and precipitation enhancement."

Location: Section 4.4, lines 409–441, Figs. 9–10, S1–S2, Table S2.

Comment 6: *Line 370: The statement is valid, but it is currently too brief and underdeveloped, given its importance. The authors should expand this discussion to more clearly articulate why a fully coupled land–atmosphere–ecosystem modeling framework is necessary for future work. In particular,* *PV installations can alter not only surface energy balance but also vegetation dynamics, soil moisture, and carbon fluxes. These processes may introduce additional feedbacks that are not captured in the current WRF-PV framework and could influence both local climate and longer-term ecosystem responses. The authors are encouraged to elaborate on (1) which key ecosystem processes are currently missing, (2) how their omission may affect the interpretation of the present results, and (3) how incorporating such processes in future model development could improve the robustness of PV–climate impact assessments. This would strengthen the discussion and better position the study within the broader context of land–climate interactions.*

Response: Thank you for this valuable suggestion. We agree that the original discussion did not sufficiently explain the need for a fully coupled land–atmosphere–ecosystem modeling framework. We have clarified that soil moisture evolved interactively in the Noah land-surface model in both WRF_CTL and WRF_PV and was therefore not held fixed. Nevertheless, the present study did not systematically diagnose the response of soil moisture.

Vegetation conditions were prescribed rather than dynamically simulated. Consequently, the present results primarily represent short-term physical responses to PV deployment and do not include longer-term vegetation-mediated feedbacks through transpiration, sensible–latent heat partitioning, and carbon exchange. We therefore identify the development of a fully coupled PV–land–atmosphere–ecosystem framework as an important direction for future work, particularly for assessing agrivoltaic applications in dryland regions.

The revised text reads:

> "The present analysis focused on surface energy balance and land–atmosphere responses. Although soil moisture evolved interactively in the Noah land-surface model, its response to PV-induced shading was not systematically diagnosed. Vegetation conditions were prescribed rather than dynamically simulated. Over longer time scales, PV-induced changes in radiation, soil moisture, and near-surface microclimate may affect vegetation activity, which could modify transpiration, sensible–latent heat partitioning, and carbon exchange (Barron-Gafford et al., 2025; Jia et al., 2026). Consequently, the present results mainly represent the short-term physical responses to PV deployment and do not fully capture these longer-term feedbacks. Therefore, future work should extend WRF-PV toward a fully coupled PV–land–atmosphere–ecosystem model that can represent indirect feedbacks through vegetation-mediated land–atmosphere exchange, thereby improving the robustness of PV–climate impact assessments. Such a framework would be useful for future agrivoltaic applications in dryland regions, where the climatic effects of panel shading are closely tied to soil moisture conservation and vegetation-mediated land–atmosphere exchange (Ruth et al., 2026)."

Location: Section 5, lines 500–510.

Comment 7: *Line 25: The introduction would benefit from a clearer articulation of the importance of PV system design in shaping climate impacts. At present, the discussion treats PV installations somewhat generically, but key design parameters, such as panel tilt angle, row spacing, orientation, tracking systems, and mounting height, strongly influence surface albedo, shading patterns, aerodynamic roughness, and heat exchange processes. These factors can modulate the magnitude and even the direction of PV-induced radiative and thermal effects.*

Response: Thank you for this helpful suggestion. We have expanded the Introduction to clarify that PV system design plays an important role in shaping the radiative and thermal effects of PV installations.

The revised text reads:

> "Key PV system design parameters, such as panel tilt angle, row spacing, orientation, tracking systems, and mounting height, strongly influence surface albedo, shading patterns, and heat exchange processes (Smith et al., 2022; Stanislawski et al., 2022). These factors can modulate the magnitude and spatiotemporal characteristics of PV-induced radiative and thermal effects (Glick et al., 2020; Zainali et al., 2023)."

Location: Section 1, lines 41–45.

Comment 8: *The references appear to be not enough. Please update the literature cited to better position the work.*

Line 32: Barron-Gafford et al. "Agrivoltaics provide mutual benefits across the food–energy–water nexus in drylands." Nature Sustainability 2.9 (2019): 848-855.

Line 370: Jia et al. "Climate-driven divergence in biophysical and economic impacts of agrivoltaics.Proceedings of the National Academy of Sciences 123.10 (2026): e2514380123.

Ruth et al. "Enhancing climate-smart crop performance in arid agrivoltaics systems: effects of photovoltaic shading and soil amendments on tepary bean growth, yield, and associated soil microbiome." Plant and Soil (2026): 1-25.

Response: Thank you for this valuable suggestion. We have expanded the literature discussion and added the suggested studies on agrivoltaic water, vegetation, and ecosystem responses, including Barron-Gafford et al. (2019), Jia et al. (2026), and Ruth et al. (2026).

Location: Sections 1 and 5, lines 36, 504, 510.

References

Barron-Gafford, G. A., Pavao-Zuckerman, M. A., Minor, R. L., Sutter, L. F., Barnett-Moreno, I., Blackett, D. T., Thompson, M., Dimond, K., Gerlak, A. K., Nabhan, G. P., and Macknick, J. E.: Agrivoltaics provide mutual benefits across the food–energy–water nexus in drylands, Nat. Sustain., 2, 848–855, https://doi.org/10.1038/s41893-019-0364-5, 2019.

Barron-Gafford, G. A., Murphy, P., Salazar, A., Lepley, K., Rouini, N., Barnett-Moreno, I., and Macknick, J. E.: Agrivoltaics as a climate-smart and resilient solution for midday depression in photosynthesis in dryland regions, Npj Sustain. Agric., 3, 32, https://doi.org/10.1038/s44264-025-00073-1, 2025.

Duffie, J. A. and Beckman, W. A.: Solar Engineering of Thermal Processes, 4th ed., John Wiley & Sons, Inc., https://doi.org/10.1002/9781118671603, 2013.

Fan, C. and Huang, X.: Direct impact of solar farm deployment on surface longwave radiation, Environ. Res. Commun., 3, 125006, https://doi.org/10.1088/2515-7620/ac40f1, 2021.

Glick, A., Smith, S. E., Ali, N., Bossuyt, J., Recktenwald, G., Calaf, M., and Cal, R. B.: Influence of flow direction and turbulence intensity on heat transfer of utility-scale photovoltaic solar farms, Sol. Energy, 207, 173–182, https://doi.org/10.1016/j.solener.2020.05.061, 2020.

Heusinger, J., Broadbent, A. M., Sailor, D. J., and Georgescu, M.: Introduction, evaluation and application of an energy balance model for photovoltaic modules, Sol. Energy, 195, 382–395, https://doi.org/10.1016/j.solener.2019.11.041, 2020.

Jia, M., Peng, B., Guan, K., Lawrence, D. M., DeLucia, E. H., Knapp, A. K., Barron-Gafford, G. A., Khanna, M., Lombardozzi, D. L., Sturchio, M. A., Kannenberg, S. A., Zhao, L., McCall, J., Tang, J., Bernacchi, C. J., Mwebaze, P., Majeed, F., Lee, D., and Time, A.: Climate-driven divergence in biophysical and economic impacts of agrivoltaics, Proc. Natl. Acad. Sci., 123, e2514380123, https://doi.org/10.1073/pnas.2514380123, 2026.

Jiang, J., Gao, X., Lv, Q., Li, Z., and Li, P.: Observed impacts of utility-scale photovoltaic plant on local air temperature and energy partitioning in the barren areas, Renew. Energy, 174, 157–169, https://doi.org/10.1016/j.renene.2021.03.148, 2021.

Li, A., Liu, L., Li, S., Cui, X., Chen, X., and Cao, X.: Global photovoltaic solar panel dataset from 2019 to 2022, Sci. Data, 12, 637, https://doi.org/10.1038/s41597-025-04985-y, 2025a.

Li, G., Hernandez, R. R., Blackburn, G. A., Davies, G., Hunt, M., Whyatt, J. D., and Armstrong, A.: Ground-mounted photovoltaic solar parks promote land surface cool islands in arid ecosystems, Renew. Sustain. Energy Transit., 1, 100008, https://doi.org/10.1016/j.rset.2021.100008, 2021.

Li, Y., Kalnay, E., Motesharrei, S., Rivas, J., Kucharski, F., Kirk-Davidoff, D., Bach, E., and Zeng, N.: Climate model shows large-scale wind and solar farms in the Sahara increase rain and vegetation, Science, 361, 1019–1022, https://doi.org/10.1126/science.aar5629, 2018.

Lin, G.: Photovoltaic dataset of China from 2013 to 2023 for ten years, https://doi.org/10.57760/sciencedb.15684, 2024.

Ruth, M., Kushwaha, P., Barron-Gafford, G. A., and Babst-Kostecka, A.: Enhancing climate-smart crop performance in arid agrivoltaics systems: effects of photovoltaic shading and soil amendments on tepary bean growth, yield, and associated soil microbiome, Plant Soil, 519, 1795–1819, https://doi.org/10.1007/s11104-025-08247-z, 2026.

Smith, S. E., Viggiano, B., Ali, N., Silverman, T. J., Obligado, M., Calaf, M., and Cal, R. B.: Increased panel height enhances cooling for photovoltaic solar farms, Appl. Energy, 325, 119819, https://doi.org/10.1016/j.apenergy.2022.119819, 2022.

Stanislawski, B. J., Harman, T., Silverman, T. J., Cal, R. B., and Calaf, M.: Row spacing as a controller of solar module temperature and power output in solar farms, J. Renew. Sustain. Energy, 14, 063702, https://doi.org/10.1063/5.0123641, 2022.

Sun, X., Silverman, T. J., Zhou, Z., Khan, M. R., Bermel, P., and Alam, M. A.: An Optics-Based Approach to Thermal Management of Photovoltaics: Selective-Spectral and Radiative Cooling, IEEE J. Photovolt., 7, 566–574, https://doi.org/10.1109/JPHOTOV.2016.2646062, 2017.

Wang, X., Zhou, Q., Zhang, Y., Liu, X., Liu, J., Chen, S., Wang, X., and Wu, J.: Diurnal Asymmetry Effects of Photovoltaic Power Plants on Land Surface Temperature in Gobi Deserts, Remote Sens., 16, 1711, https://doi.org/10.3390/rs16101711, 2024.

Xu, Z., Li, Y., Qin, Y., and Bach, E.: A global assessment of the effects of solar farms on albedo, vegetation, and land surface temperature using remote sensing, Sol. Energy, 268, 112198, https://doi.org/10.1016/j.solener.2023.112198, 2024.

Yang, Y., Lin, S., Lu, R., and Liu, X.: CPVPD-2024: A Chinese photovoltaic plant dataset derived via a topography-enhanced deep learning framework, Sci. Data, 12, 1601, https://doi.org/10.1038/s41597-025-05891-z, 2025.

Ying, J., Li, Z., Yang, L., Jiang, Y., Luo, Y., and Gao, X.: The characteristics and parameterizations of the surface albedo of a utility-scale photovoltaic plant in the Gobi Desert, Theor. Appl. Climatol., 151, 1469–1481, https://doi.org/10.1007/s00704-022-04337-5, 2023.

Zainali, S., Ma Lu, S., Stridh, B., Avelin, A., Amaducci, S., Colauzzi, M., and Campana, P. E.: Direct and diffuse shading factors modelling for the most representative agrivoltaic system layouts, Appl. Energy, 339, 120981, https://doi.org/10.1016/j.apenergy.2023.120981, 2023.

Zhang, J., Wu, L., and Dong, W.: Land-atmosphere coupling and summer climate variability over East Asia, J. Geophys. Res., 116, D05117, https://doi.org/10.1029/2010JD014714, 2011.

Zhang, X. and Xu, M.: Assessing the Effects of Photovoltaic Powerplants on Surface Temperature Using Remote Sensing Techniques, Remote Sens., 12, 1825, https://doi.org/10.3390/rs12111825, 2020.